Nuclear Engineering and Technology 55 (2023) 3692–3699

Contents lists available at ScienceDirect

Nuclear Engineering and Technology

journal homepage: www.elsevier.com/locate/net

Original Article

Design and fabrication of beam dumps at the μSR facility of RAON for high-energy proton absorption

Jae Chang Kim [a], Jae Young Jeong [a], Kihong Pak [a], Yong Hyun Kim [a], Junesic Park [b], Ju Hahn Lee [c], Yong Kyun Kim [a, *]

[a] Department of Nuclear Engineering, Hanyang University, Seoul, 04763, Republic of Korea
[b] Korea Atomic Energy Research Institute (KAERI), Daejeon, 34057, Republic of Korea
[c] Moeemotion, Pohang, 37673, Republic of Korea

ARTICLE INFO

Article history:
Received 5 February 2023
Received in revised form
17 May 2023
Accepted 20 June 2023
Available online 20 June 2023

Keywords:
Beam dump
Particle accelerator
Muon facility
μSR
Monte Carlo simulation
Structure analysis

ABSTRACT

The Rare isotope Accelerator complex for ON-line experiments in Korea houses several accelerator complexes. Among them, the μSR facility will be initially equipped with a 600 MeV and 100 kW proton beam to generate surface muons, and will be upgraded to 400 kW with the same energy. Accelerated proton beams lose approximately 20% of the power at the target, and the remaining power is concentrated in the beam direction. Therefore, to ensure safe operation of the facility, concentrated protons must be distributed and absorbed at the beam dump. Additionally, effective dose levels must be lower than the legal standard, and the beam dumps used at 100 kW should be reused at 400 kW to minimize the generation of radioactive waste. In this study, we introduce a tailored method for designing beam dumps based on the characteristics of the μSR facility. To optimize the geometry, the absorbed power and effective dose were calculated using the MCNP6 code. The temperature and stress were determined using the ANSYS Mechanical code. Thus, the beam dump design consists of six structures when operated at 100 kW, and a 400 kW beam dump consisting of 24 structures was developed by reusing the 100 kW beam dump.

1. Introduction

The Rare isotope Accelerator complex for ON line experiments (RAON) is a multifaceted accelerator facility that houses several specialized instruments, including the KOrea Broad acceptance Recoil spectrometer and Apparatus (KOBRA), Beam Irradiation System (BIS), and Muon Spin Rotation/Relaxation/Resonance (μSR) facility [1]. The μSR facility uses surface muons generated by a 600 MeV proton beam interacting with a graphite target to conduct materials science experiments, as illustrated in Fig. 1 [2]. However, only approximately 20% of the beam power is used for muon production, while the remaining energy continues past the graphite target. Therefore, a beam dump is necessary to safely absorb the remaining energy, considering the unique characteristics of the μSR facility.

Beam dump, which is a critical safety component in accelerator facilities, utilize high-energy particles, and each facility customizes its beam dump to fit its specific needs. For example, the Hadron Hall of J-PARC in Japan employs a beam dump with a conical hole to absorb 50 GeV protons [3], while PSI in Switzerland uses a beam dump with a cylindrical hole to absorb 590 MeV protons [4]. At KOMAC in Korea, a beam dump with two wedge-shaped plates absorbs 20 MeV protons [5]. **FRIB** in the USA employs a rotating beam dump made of alloys and water to absorb heavy ions at an energy of 200 MeV/u [6]. The design of each beam dump is specific to the characteristics of each facility, including the energy, beam power, and shape of the incident particles.

The μSR facility is initially planned to operate a beam power of 100 kW (165 pμA, 600 MeV), with an eventual upgrade to 400 kW (660 pμA, 600 MeV). Therefore, the beam dump installed for the 100 kW beam power must be reusable for the 400 kW beam power to minimize radioactive waste. As the beam dump will become radioactive after absorbing the beam, accessing it during operation will be difficult for workers. Thus, a design that minimizes maintenance is essential. Additionally, the beam dump must be capable of absorbing the beam without a defocusing device after the graphite target, as beam dump must be installed within a limited space surrounded by concrete blocks, as shown in Fig. 1. Furthermore, it should be designed to limit the effective dose rate to 5 μSv/h in the worker area.

* Corresponding author.
E-mail address: ykkim4@hanyang.ac.kr (Y.K. Kim).

https://doi.org/10.1016/j.net.2023.06.034

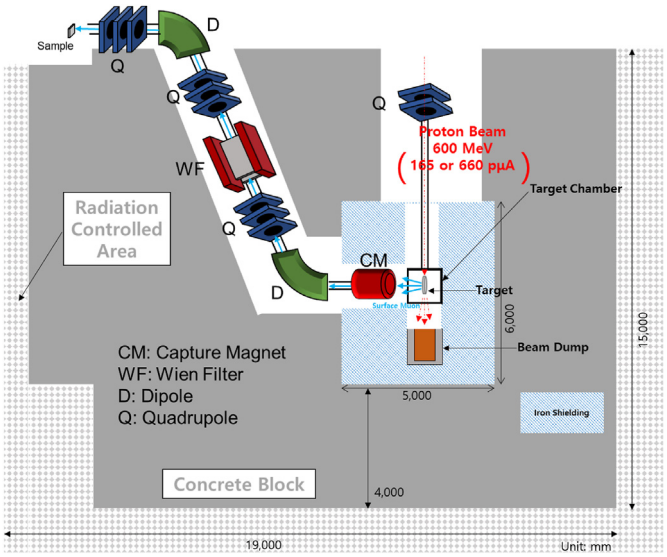

Fig. 1. μSR facility at RAON.

In this study, we introduce the design method of beam dump that meets the requirements of the μSR facility. We first determined the shape and material of the beam dump, and then calculated the behavior of protons, absorbed energy in the beam dump, and **effective dose using MCNP6**, a Monte Carlo method-based particle transport code [7]. We also assessed the temperature of the beam dump and the stress caused by thermal expansion using **ANSYS Mechanical 2021 R1**, a finite element analysis code. Finally, we present the designs of 100 kW and 400 kW beam dumps, which meet the requirements of the μSR facility, designed using computational simulation codes.

2. Selection of design criteria

2.1. Proton beam behavior near graphite target

The graphite target used in the beam dump design was configured as shown in Fig. 2, with a cylindrical shape and dimensions of 400 mm outer diameter, 300 mm inner diameter, and 5 mm thickness. The final design incorporated structures for rotation, slits, and holes to reduce stress due to thermal expansion [8]. The incident protons on the graphite target were accelerated to 600 MeV, following a normal distribution, as illustrated in Fig. 2. **The root mean square beam sizes at the target were 1.163 mm (horizontal) and 2.879 mm (vertical), while the corresponding root mean square angular divergences were 0.1232 mrad (horizontal) and 0.3695 mrad (vertical).** To investigate the behavior of protons that pass through the target, simulations were performed using the MCNP6 code. Assuming azimuthal symmetry and z-axis beam direction, the beam power was defined as the product of energy and number of protons. The resulting polar angle-dependent distribution of beam power is presented in Fig. 2.

The simulation results showed that only approximately 10% of the incident beam power was absorbed in the graphite target, with another 10% used to break the binding energy or convert it into other forms of radiation. The remaining 80% of the power passed through the target, with 90% of that power concentrated within a 10° polar angle and 60% concentrated within 1°. Therefore, at an operational beam power of 100 kW, a significant portion (47 kW) of the power is concentrated on a small 10 cm^2 surface located at a distance of 1 m from the target. To effectively absorb the beam power, the beam dump structure must properly distribute the concentrated power.

2.2. Determination of the beam dump structure

Various types of beam dumps exist to disperse and absorb high heat fluxes. For instance, the beam dump used in **FRIB** is a structure that consists of a shell made of Ti–6Al–4V, inside which coolant circulates continuously while the entire device rotates. However, this method is not suitable for the μSR facility. While **FRIB** uses 200 MeV/u ion beams with a short Continuous Slowing Down Approximation(CSDA) range in water, the μSR facility uses 600 MeV proton beams with a longer CSDA range. This leads to larger beam dumps, making them difficult to use in limited spaces and requiring additional maintenance owing to various rotating structures. Therefore, the facility did not adopt the **FRIB** method. Beam dumps used in KOMAC, J-PARC, and PSI disperse and absorb beams through a physical collimator structure without any moving device. KOMAC uses an electromagnet installed in front of the beam dump to spread the beam initially, followed by a wedge-shaped beam

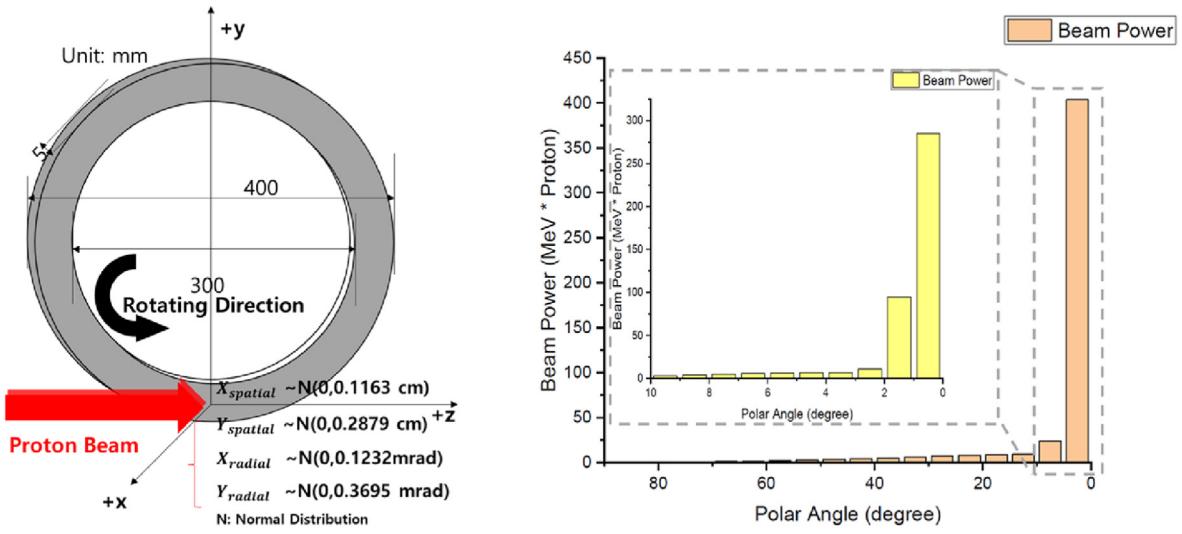

Fig. 2. Proton behavior near the graphite target.

dump with two plates. However, in the μSR facility, it is difficult to install an electromagnet to defocus the beam owing to spatial constraints, particularly when the beam is focused in both x and y directions, making it impossible to use a wedge-shaped beam dump. In the case of the Hadron Hall in J-PARC, the incoming beam to the beam dump is defocused by the target, resulting in a beam size of 400 mm in diameter at the entrance of the beam dump [9]. To safely absorb this defocused beam, a conical hole with a diameter of 330 mm and a height of 4 m was utilized in the beam dump [10]. However, in the μSR facility, the incoming beam to the beam dump is not sufficiently defocused. Therefore, a smaller angle and more space is required if a conical hole is used. Consequently, the engineering and practical constraints prevent the use of conical holes in the μSR facility beam dump. The beam dump structure chosen for this study is based on the design of the beam dump used in SINQ of PSI, as shown in Fig. 3.

The beam dump of the μSR facility consists of a collimator-type component (CTC) with a cylindrical central hole and normal-type component (NTC) that finally absorbs the beam. The CTC is used to partially absorb protons with a relatively large emission angle. Therefore, the central hole is larger closer to the incident beam, and smaller closer to the NTC. This structure has the advantage of reusing existing components by installing additional CTC when the beam power of the facility is upgraded. Additionally, the hexahedral structure was chosen, unlike PSI, which allows for alignment and operation while using relatively few structures **along with good machinability**.

In this beam dump structure, heat generated by protons is concentrated at the center while cooling is performed at the edge using a coolant. Thus, a material with high thermal conductivity is necessary for efficient heat removal. Various materials with high thermal conductivity, such as silver, carbon allotropes, and copper, exist, but copper is the most suitable, considering the cost and manufacturability. Among various copper alloys, C10200, also known as oxygen-free copper, is a type of copper with an oxygen content of less than 10 ppm, and exhibits high thermal conductivity and strong hydrogen brittleness. C10200 has already been successfully employed in various facilities, and thus chosen as the material for the beam dumps. Consequently, we established the design criteria for the temperature and stress of the beam dump below the softening point (200 °C) and yield stress (69 MPa) of C10200, respectively. Table 1 provides the material properties of the C10200 used in the simulation [11–13].

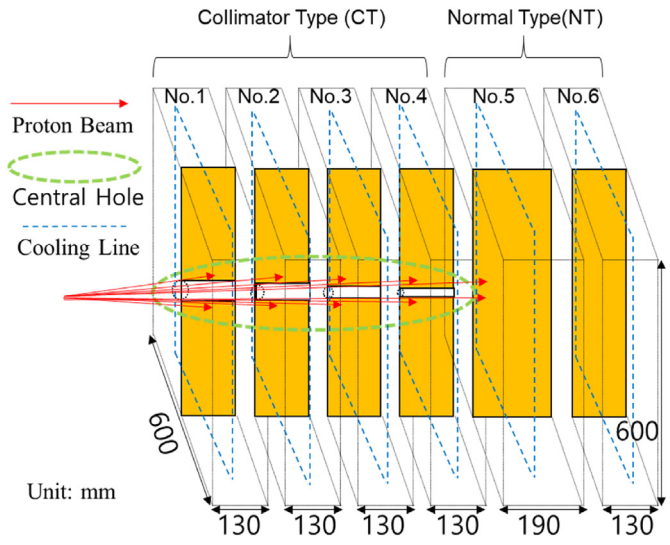

Fig. 3. Structure of the 100 kW beam dump.

2.3. Determination of beam dump size and number

During operation, the irradiation exposes the beam dump and results in activation and the generation of radioactive waste. Therefore, the beam dump size should be minimized while acquiring safety requirements. Additionally, a smaller beam dump allows the installation of more shielding bodies as the beam dump and iron shielding are constrained in a limited space. The size of the beam dump in this study was determined using MCNP6. The CSDA range of a 600 MeV proton incident on copper at a density of 8.96 g/cm^3 is 25 cm [14]. Although the energy of protons past the graphite target is less than 600 MeV, 600 MeV protons were conservatively simulated to be incident on a virtual cylinder-shaped beam dump with a radius of 60 cm and height of 100 cm, which was sufficiently larger than the CSDA range, as shown in Fig. 4. The absorbed energy was calculated by dividing the virtual beam dump into 1 cm intervals in each direction, and the size of the beam dump was determined as the region in which 0.1% of the total absorption energy was absorbed. Therefore, the required size was determined to be 32 cm in the beam penetration direction and 21 cm in the vertical direction, as shown in Fig. 4.

The CTC has a central hole, and all components are equipped with coolants flowing at the edge. The vertical size of the component was determined to be 30 cm, considering the cooling water position and radius of the central hole. **In consideration of the requirement for partial absorption of proton power, it was necessary to ensure that the thickness of each component remained smaller than the CSDA range (25 cm).** Therefore, the thickness of each component was determined to be 13 cm, **which was the most economical at the time of design and was smaller than CSDA range,** and an NTC with a thickness of 19 cm was added to meet the required size of 32 cm in the beam penetration direction. The absorbed power in the beam dump was evaluated to be approximately 60 kW when the facility operated at a beam power of 100 kW. To absorb approximately 10 kW of power at each component, a 100 kW beam dump was designed to consist of four CTCs ($60 \times 60 \times 13$ cm^3) and two NTCs ($60 \times 60 \times 13$ cm^3) and ($60 \times 60 \times 19$ cm^3). Fig. 3 shows the CTC closest to the beam as No. 1 and the NTC farthest from the beam as No. 6.

3. Optimization method of beam dump

3.1. Optimization objectives and procedure

The 100 kW beam dump design was optimized in three ways: the size of the central hole in the CTC was adjusted to prevent hotspots generated in the NTC by the concentrated proton beams

Table 1
Material properties of C10200.

Density	Thermal expansion	Young's modulus	Poisson's ratio	Thermal conductivity	Yield strength	Softening temperature
[g/cm3]	[1/K]	[MPa]	[–]	[W/m K]	[MPa]	[°C]
8.96	1.77×10^{-5}	1.17×10^{5}	0.33	374–391	69	200

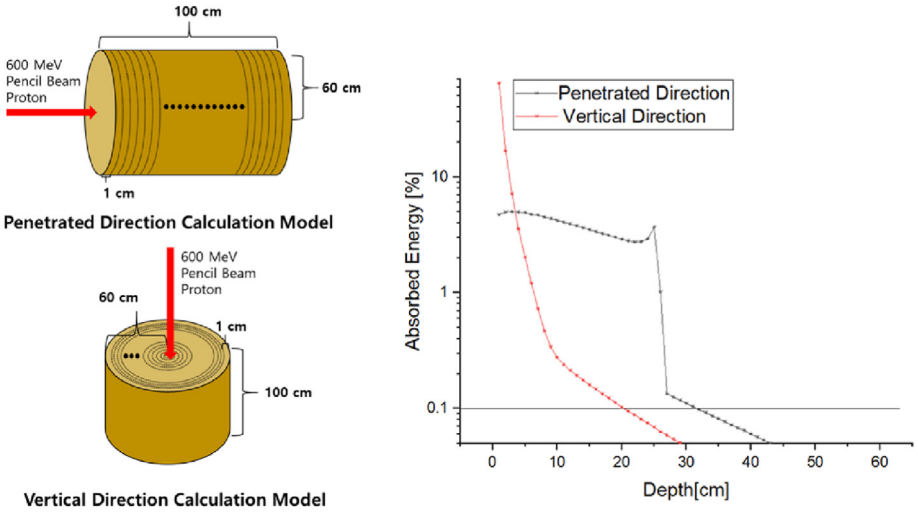

Fig. 4. Simulation geometry and results for size determination.

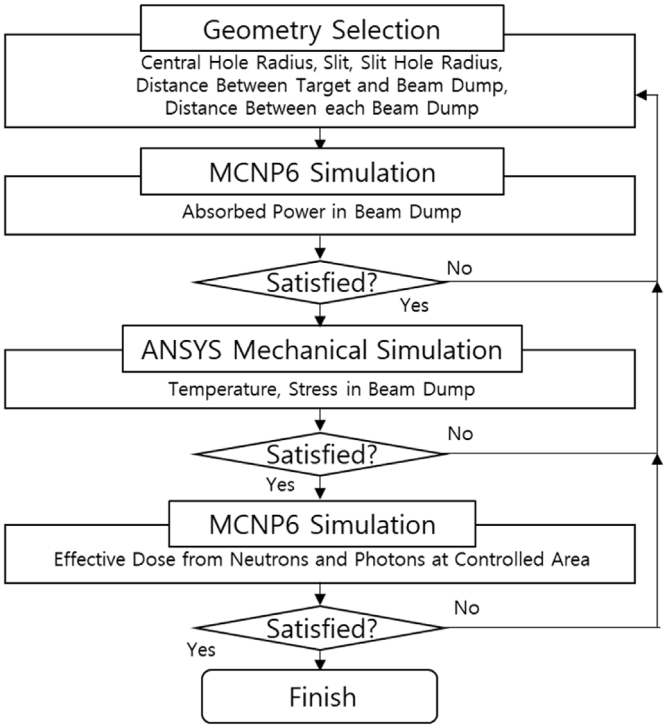

Fig. 5. Beam dump geometry and optimization procedure.

passing through the collimator, the geometries of the slits were optimized to prevent thermal stress, and the position and interval of the components were adjusted to maintain the effective dose in the controlled area below the design goals. Fig. 5 shows the three-step optimization procedure for the beam dump. The absorbed power at each component was calculated using MCNP6 in the initial geometry. Then, temperature and thermal stress of each component were evaluated using ANSYS Mechanical. Finally, **the effective dose from neutrons and photons** in the controlled area was calculated using MCNP6. If the design goals were unsatisfied at any stage, the same procedure was repeated by modifying the initial geometry. After designing the 100 kW beam dump, the 400 kW beam dump was designed by reusing the 100 kW beam

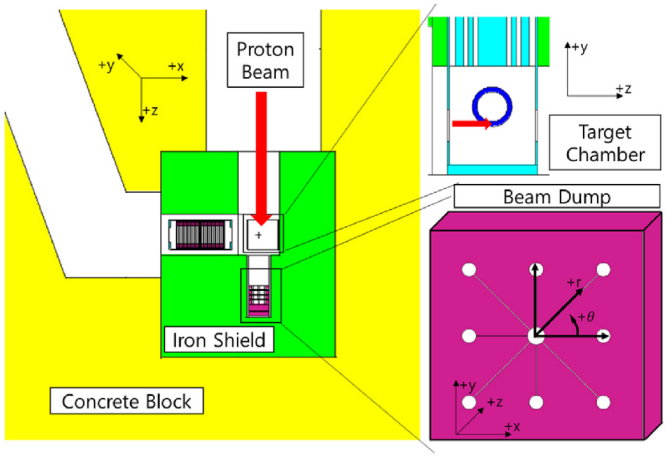

Fig. 6. MCNP6 simulation geometry.

dump and optimizing the location and size of the central hole by adding 18 CTCs. The same optimization procedure was followed for the **400 kW** beam dump without dose calculation owing to the construction plan of a new shielding facility for the upgraded beam power.

3.2. MCNP6 simulation

The absorbed power in the component was evaluated using MCNP6 with the geometry shown in Fig. 6. A 600 MeV proton beam with a normal distribution shown in Fig. 2 was used as the source term for the simulation. The absorbed energy in the beam dump is not only affected by the proton beam but also by various particles generated from reactions such as spallation in the graphite target. Therefore, to account for this, we simulated the radiation produced when a 600 MeV proton interacts with graphite or copper using MCNP6. Therefore, 16 transported particles, including protons, neutrons, and heavy ions, were found to have significant production, and these were selected to be transported in simulations. The absorbed power at the beam dump was calculated by evaluating the energy absorbed by these transported particles in a space divided into 1 cm intervals for r, z, and $\theta = 45^\circ$ intervals ($1\ \text{cm} \times 1\ \text{cm} \times 45^\circ$, $r \times z \times \theta$), as shown in Fig. 6. The design goal of

the absorbed power was to ensure that each collimator type absorbs approximately 10 kW, with a decreasing absorbed power from the first CTC to the last CTC. This is because the radius of the central hole decreases as it gets farther from the beam, thus reducing the cooling performance.

The effective dose from neutrons and photons in the controlled area was calculated using MCNP6 with the geometry shown in Figs. 1 and 6. The source term was utilized in the simulation to improve computational efficiency. The source term was produced by dividing the neutrons generated in the beam dump and graphite target into polar angles of 0–90° with a 5° interval and 90–180° with a 10° interval and dividing the energy into 100 logarithmic intervals from 1 keV to 600 MeV, in the geometry used to simulate absorbed power. **During the calculation of the source term, the power of generated photons was evaluated to be approximately 2.2% compared to neutrons. Additionally, the maximum energy of generated photons was estimated to be around 13 MeV. The half-value layer of 15 MeV photons in ordinary concrete was approximately 15 cm [15]. As a result, the influence of photons was considered negligible Therefore, only neutrons were taken into account in the source term, while both neutrons and photons were transported in the simulations.** The effective dose was calculated using the effective dose conversion coefficient of the anterior–posterior (AP) in ICRP74, and the controlled area was calculated by dividing volume into a mesh of 30 × 30 × 30 cm^3. **The final effective dose was determined by summing the effective dose from both neutrons and photons.** The design goal was to ensure that the maximum dose rate was less than 5 μSv/h.

3.3. ANSYS mechanical simulation

An ANSYS thermal analysis was used to calculate the temperature of the beam dump. For the heating condition within the beam dump, we assumed that 100% of the absorbed power calculated through MCNP6 was converted into heat. Therefore, the geometry used in MCNP6 simulations was modeled in ANSYS, and the absorbed power in the beam dump, calculated at intervals of 1 cm × 1 cm × 45°, was converted into internal heat generation using ANSYS APDL. The cooling condition was assumed to consist only of forced convection **by liquid water** in the cooling line, as shown in Fig. 7, except radiation and natural convection. Each cooling line is cylindrical with a radius of 1.5 cm. The No. 5 dump has four cooling lines, while the other five components have two per component. Water is used as the coolant, **with a velocity of 0.3 m/sec for the No. 5 dump and 0.2 m/sec for the other components. The inlet temperature of the coolant for all components is 22°C.**

The Gnielinski correlation, shown in Eq. (1), was used to derive the heat transfer coefficient from the surface of each cooling line [16].

$$Nu_D = \frac{\left(\frac{f}{8}\right)(Re_D - 1000)Pr}{1 + 12.7\left(\frac{f}{8}\right)^{\frac{1}{2}}\left(Pr^{\frac{2}{3}} - 1\right)}, f = (0.79\,ln(Re_D) - 1.64)^{-2} \quad (1)$$

Eq. (1) is valid for $3000 < Re_D < 5.0 \times 10^6$ and $0.5 < Pr < 2000$. For all cooling lines of the components, the Prandtl number (Pr) was approximately 7. The Reynolds number (Re_D) was 8970 for the No. 5 dump and 5980 for the other components. Therefore, under the condition that Eq. (1) is satisfied, the Nusselt Number (Nu_D) was calculated. The heat transfer coefficient on the cooling water surface was calculated to be 1400 W/m^2K at the No. 5 dump and 1000 W/m^2K at the other components. Therefore, the temperature was calculated using internal heat generation and forced convection, and the design goal was to ensure that the maximum temperature of each component was below 200 °C. The stress of each component owing to thermal expansion was calculated using the ANSYS structural analysis. The maximum von Mises stress was calculated using the previously calculated temperature of each component as an input value. Particularly, the stress above the design goal occurred near the central hole of the CTC, and to solve this problem, we optimized the number of slits and size of the slit holes, as shown in Fig. 7. The design goal of stress in all components was aimed to be below the yield strength (69 MPa) of copper.

4. Design result and discussion

During the optimization of the 100 kW beam dump, we encountered two main challenges. The first was the evaluation of temperature above 200 °C in the No. 5 dump owing to an excessive amount of absorbed power. To address this issue, we explored various options to reduce the absorbed power or enhance the cooling performance. Possible methods included reducing the size of the central hole, moving the 100 kW beam dump away from the target, or reducing the thickness of the No. 5 dump. However, these methods also posed some challenges, such as fabrication and alignment issues or high-dose problems in the controlled area. Moreover, decreasing the thickness of the No. 5 dump may not

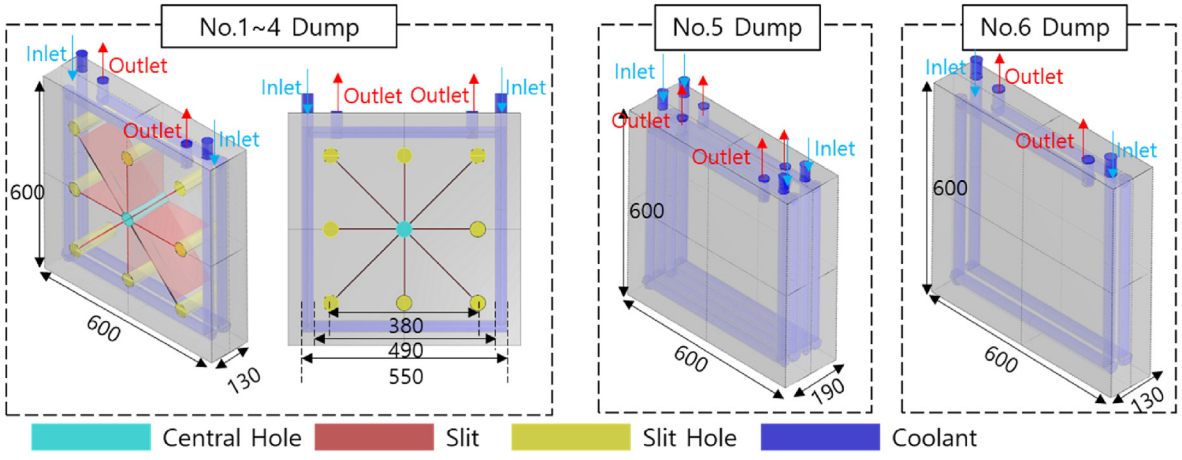

Fig. 7. ANSYS calculation geometry.

Table 2
Stress evaluation with varying slit radius and number of slits.

Slit radius	Number of slit		
	2	4	8
0.5 cm	216 MPa	118 MPa	58 MPa
1 cm	156 MPa	92 MPa	45 MPa
1.5 cm	128 MPa	73 MPa	35 MPa
2 cm	108 MPa	55 MPa	31 MPa
2.5 cm	101 MPa	47 MPa	23 MPa
3 cm	101 MPa	42 MPa	22 MPa

necessarily reduce the absorbed power per volume, as shown in Fig. 4, when the traveling distance of 600 MeV protons in copper is shorter than the Bragg peak. Therefore, we opted for a relatively thick No. 5 dump and installed as many coolant lines as possible, while using the maximum flow rate available in the μSR facility to lower the temperature of the No. 5 dump.

The second challenge we faced was the evaluation of thermal stress near the central hole of the collimator, which exceeded our design objective. To mitigate this issue, we added a slit, as depicted in Fig. 7, to provide a space for expansion. However, we encountered the same problem at the end of the slit, so we added a cylindrical slit hole to address it. We chose a thickness of 2 mm for the slit, as it was the smallest size that is economically feasible while providing adequate expansion space. To maintain symmetry, we determined that the CTC should have an even number of slits. Additionally, we varied the number of slits and the radius of the slit hole to simulate the stress of the No. 4 dump, as presented in Table 2. Because the maximum stress occurred on the surface of the central hole or slit hole, rather than inside the structure, we set the design goal to be half the yield stress for the CTC. Eventually, we determined that eight slits and a slit-hole radius of 2 cm were optimal for the CTC.

Fig. 8 illustrates the temperature and stress distribution of the optimized 100 kW beam dump, consisting of four CTCs and two NTCs, located 148 cm away from the graphite target, with a distance of 1 cm between each component. The maximum temperature and stress were evaluated to be 142.6 °C and 58.6 MPa, respectively, at the No. 5 dump. As shown Fig. 8, the CTCs exhibited the maximum temperature near the central hole and maximum stress near the slit hole. Similarly, the NTCs exhibited the maximum temperature on the surface exposed to the beam, while the maximum stress was evaluated inside each component. **The maximum volumetric heat density was positioned at the points of contact between the beam and each dump components.** The 100 kW beam dump satisfied the design objectives. Table 3 provides the absorbed power, maximum temperature, maximum stress, central hole size, **outlet coolant temperature, and maximum volumetric heat density** of each beam dump.

Fig. 9 illustrates the results of the effective dose calculation of the μSR facility. To meet the effective dose requirements in the shielding structure shown in Fig. 1, the distance between the beam dump and target must be reduced. However, decreasing the distance necessitates a smaller central hole for the CTC and increases the absorption dose of the solenoid. Given the practical limitations of fabrication errors, alignment, and solenoid design lifetime, constructing an additional concrete shield with a thickness of 800 mm was deemed necessary. Thus, **the maximum effective dose in all controlled areas was evaluated to be below the target**

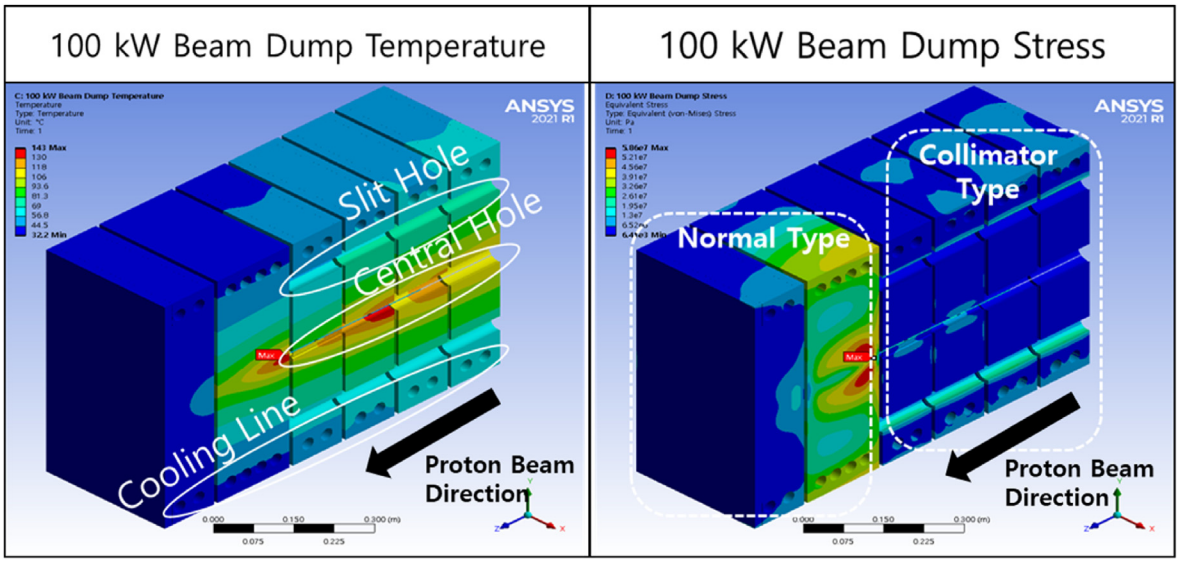

Fig. 8. Temperature and stress distribution of 100 kW beam dump.

Table 3
Optimization results of 100 kW beam dump.

Beam dump number	Absorbed power [kW]	Max temperature [°C]	Max stress [MPa]	Central hole radius [cm]	Outlet coolant temperature [°C]	Max volumetric heat density [W/cm^3]
1	13.2	115.2	27.3	2.5	33.2	15.8
2	11.8	125.8	27.0	2.1	32.0	28.8
3	11.1	139.7	25.7	1.3	31.4	55.1
4	8.7	128.3	24.0	0.7	29.4	39.0
5	13.6	142.6	58.6	–	25.8	128.9
6	1.9	55.5	16.5	–	23.6	20.4

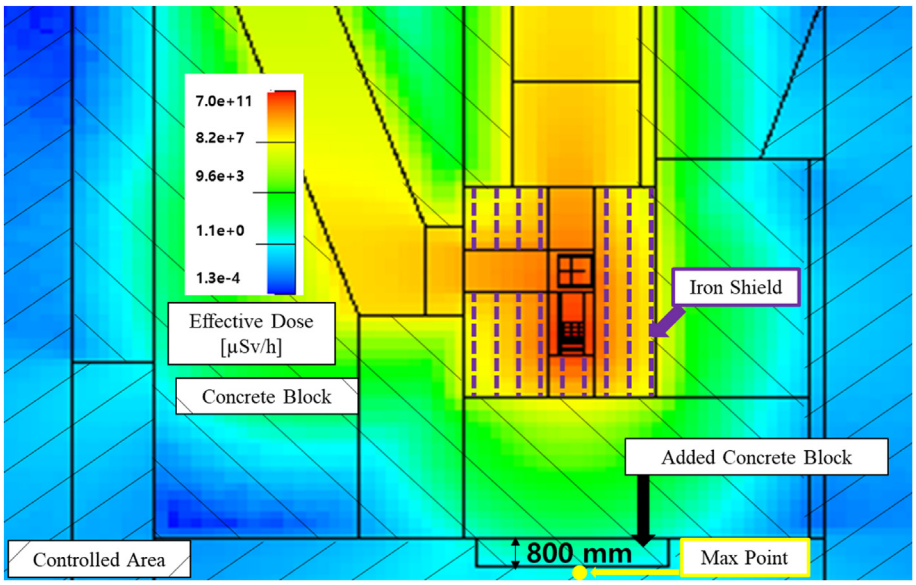

Fig. 9. Effective dose map of μSR facility.

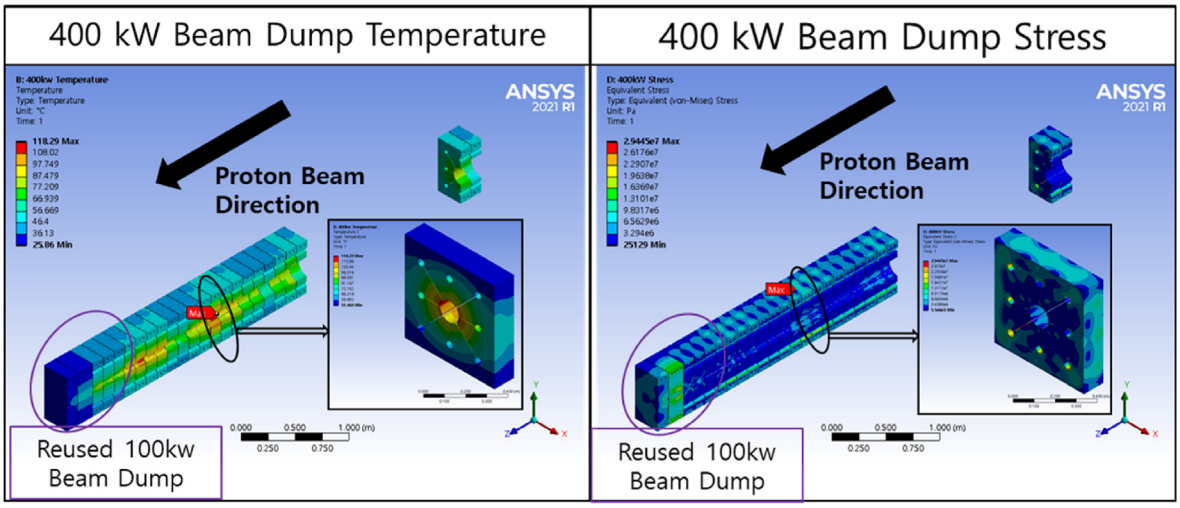

Fig. 10. Temperature and stress distribution of 400 kw beam dump.

value of 5 μSv/h (neutron: 2.09 μSv/h, photon: 0.79 μSv/h), as presented in Fig. 9.

The 400 kW beam dump was composed of 22 CTCs and 2 NTCs, as depicted in Fig. 10. The first two CTCs were installed 148 cm from the graphite target to absorb protons at a large emission angle, whereas the remaining 20 CTCs were located 376 cm away. The final six components of the 400 kW beam dump reused the 100 kW beam dump. As mentioned earlier, the existing shielding facility would be demolished and replaced with a new shielding structure upon upgrading the beam power to 400 kW. The maximum temperature and stress at the No. 11 dump were evaluated to be 118.3 °C and 29.4 MPa, respectively, when the front-most component was designated as No. 1 and the last component as No. 24.

5. Conclusion

In this study, we presented a method for designing beam dumps for the μSR facility at RAON for 100 and 400 kW beam power. The need for beam dispersion was confirmed by evaluating the proton behavior while passing through the graphite target. We selected a collimator-type structure with a central hole and used C10200 for the beam dump to achieve high thermal conductivity. Using MCNP6 and ANSYS Mechanical, we optimized the size and position of the central hole, slit, and slit hole. The maximum stress (100 kW: 58.6 Mpa; 400 kW: 29.4 MPa) and temperature (100 kW: 142.6 °C; 400 kW: 118.3 °C) in all components were evaluated to be lower than the yield strength (69 MPa) and its softening point (200 °C) of C10200, respectively. A 100 kW beam dump with a mobile structure was manufactured and installed in the μSR facility based on the design, as shown Fig. 11. **Based on the conducted experimental results of circulating coolant through the installed beam dump with a manifold connection, it was confirmed that the designed flow rate was achieved when using a pressure of 5 bar.** In the future, computational simulations and experimental results will be compared and verified while gradually increasing the beam power. When the beam power of the facility is upgraded to 400 kW, the

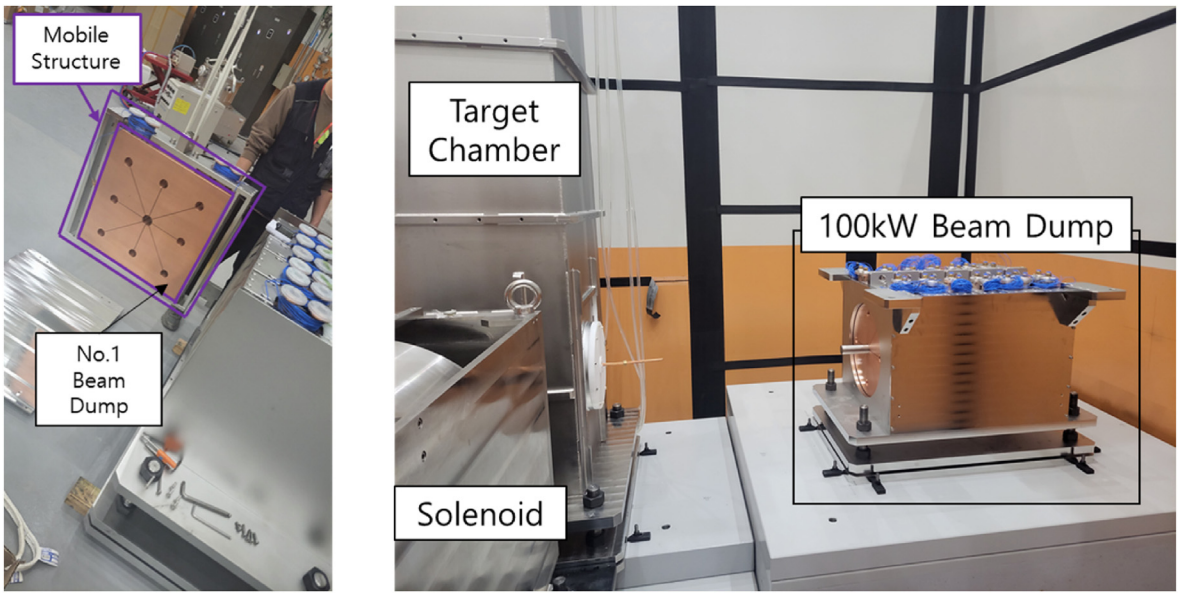

Fig. 11. Fabrication picture of 100 kW beam dump.

existing beam dump will be reused, and an additional 400 kW beam dump will be constructed and operated.

Declaration of competing interest

The authors declare that they have no known competing financial interests or personal relationships that could have appeared to influence the work reported in this paper.

Acknowledgement

This work was supported by the Rare Isotope Science Project of the Institute for Basic Science funded by the Ministry of Science and ICT and the NRF of Korea (2013M7A1A1075764).

References

[1] Y.J. Kim, Current status of experimental facilities at RAON, Nucl. Instrum. Methods Phys. Res. Sect. B Beam Interact. Mater. Atoms 463 (2020) 408–414.
[2] Kihong Pak, et al., Beam line design and beam transport calculation for the μSR facility at RAON, Nucl. Eng. Technol. 53 (10) (2021) 3344–3351.
[3] K. Agari, et al., Development and construction of the beam dump for J-PARC hadron Hall, in: Proceedings of the 2nd International Particle Accelerator Conference (IPAC), San Sebastian, Spain, 2011, September, pp. 1608–1610.
[4] I.W. D'haeseleer, Designing a Beam Dump for a 600 MeV Myrrha Linear Proton Accelerator, 2011.
[5] Jiho Kim, et al., Design of a high energy proton beam dump for KOMAC, Nucl. Instrum. Methods Phys. Res. Sect. A Accel. Spectrom. Detect. Assoc. Equip. 562 (2) (2006) 997–1000.
[6] Mikhail Avilov, et al., Thermal, mechanical and fluid flow aspects of the high power beam dump for FRIB, Nucl. Instrum. Methods Phys. Res. Sect. B Beam Interact. Mater. Atoms 376 (2016) 24, 2.
[7] Los Alamos Scientific Laboratory Group, MCNP: a general Monte Carlo code for neutron and photon transport. https://mcnp.lanl.gov/. December 2022.
[8] Jae Young Jeong, et al., Search Prospects for Axion-like Particles at Rare Nuclear Isotope Accelerator Facilities, 2022 arXiv preprint arXiv:2207.02223.
[9] K. Agari, et al., Design and R&D status of NP-hall beam dump in J-PARC, in: Proceedings, 2003, November.
[10] K. Agari, et al., Primary proton beam line at the J-PARC hadron experimental facility, Progress of Theoret. Experim. Phys. 2012 (1) (2012).
[11] D. Chapman, High Conductivity Copper for Electrical Engineering, 122, Copper Development Association's resource library, 2016, pp. 1–32.
[12] J.R. Davis (Ed.), Copper and Copper Alloys, ASM international, 2001.
[13] K.H. Tanaka, et al., J-PARC high-intensity proton accelerator facilities, nuclear and particle physics facility construction group, hadron beam line subgroup, technical design report 3, KEKInternal (August 2007), 2007-1.
[14] M.J. Berger, et al., ESTAR, PSTAR, and ASTAR: computer programs for calculating stopping-power and range tables for electrons, protons, and helium ions. http://physics.nist.gov/Star/, 2017. December 2022.
[15] J. Hubbell, S. Seltzer, Tables of X-ray mass attenuation coefficients and mass energy-absorption coefficients 1 keV to 20 MeV for elements Z = 1 to 92 and 48 additional substances of dosimetric interest. http://physics.nist.gov/PhysRefData/XrayMassCoef/cover.html, 1995. (Accessed 16 May 2023). http://physics.nist.gov/PhysRefData/XrayMassCoef/cover.html [online].
[16] T.L. Bergman, T.L. Bergman, F.P. Incropera, D.P. Dewitt, A.S. Lavine, Fundamentals of Heat and Mass Transfer, John Wiley & Sons, 2017.